

Article

Electrodeposition of ZnO/Cu₂O Heterojunctions on Ni-Mo-P Electroless Coating

Nelly Maria Rosas-Laverde ¹, Alina Iuliana Pruna ^{2,3,*} , Jesus Cembrero ³
and David Busquets-Mataix ³

¹ Department of Materials, Escuela Politécnica Nacional, Quito 170524, Ecuador; nelly.rosas@epn.edu.ec

² Center for Surface Science and Nanotechnology, Polytechnic University of Bucharest, 060042 Bucharest, Romania

³ Institute of Materials Technology, Universitat Politècnica de València, 46022 Valencia, Spain; jcembrer@mcm.upv.es (J.C.); dbusquets@mcm.upv.es (D.B.-M.)

* Correspondence: ai.pruna@gmail.com

Received: 25 August 2020; Accepted: 27 September 2020; Published: 29 September 2020



Abstract: Electroless Ni-Mo-P coatings were deposited onto ceramic tiles in order to be employed as electrodes for the electrodeposition of ZnO and Cu₂O heterojunction layers. Varying conditions, such as duration, annealing of the electroless coating and applied potential, and duration for ZnO electrodeposition were studied in order to optimize the properties of the ZnO/Cu₂O heterojunctions toward improved photoelectrical performance. The coatings were evaluated in terms of morphology, crystalline structure, and by electrochemical and photoelectrical means. The obtained results indicated that a prolonged annealing treatment at low temperature is beneficial to improve the roughness and electrical conductivity of the Ni-Mo-P coating to further enhance the electrodeposition of ZnO. The morphology analysis revealed continuous and homogeneous Ni-Mo-P coatings. The formation of cube-like Cu₂O crystals with larger grain size was induced by increasing the deposition duration of ZnO. The properties of ZnO layer are much improved when a higher cathodic potential is applied (−0.8 V) for 1 h, resulting in optimum photoelectric parameters as 1.44 mA·cm^{−2} for the J_{SC} and 760.23 μV for the V_{OC} value, respectively, for the corresponding heterojunction solar cell.

Keywords: electroless coating; Ni-Mo-P; ceramic substrate; electrodeposition; ZnO; Cu₂O

1. Introduction

Ceramic materials show excellent chemical stability, high hardness and wear resistance, and have higher melting temperature in comparison to other materials [1,2]. Owing to these properties, ceramic materials are employed in various fields such as heat exchangers, motor parts, electrical and electronic components, implants [1], as well as in electrical [3] and power electronic systems [4], as mechanical supports [5], and building-integrated photovoltaics (BIPV) [6].

The ceramics show an important drawback in some applications, namely they are poor conductors of electricity and heat and they exhibit high fragility [2]. In this regard, surface modification by methods including electroless deposition (ED) attracted attention in order to improve the electrical properties of these non-conductive surfaces (polymer, ceramics) without using external current [7–10]. The ED involves the following steps: (i) surface treatment, (ii) catalytic activation, (iii) electroless process, and (iv) annealing treatment [11]. The deposition bath is formed by a metal salt, a complexing and reducing agent, a stabilizer, an inhibitor, and others (pH regulators, wetting and polishing agents) [11,12]. Factors such as temperature, time, pH, and chemical composition directly influence the morphology, composition, and final structure of electroless coating, as well as the electrical and magnetic properties [12–14]. For example, thickness and size grain dependence were observed with

immersion duration of the substrate in the deposition bath [15]; pH has a direct relation with the reaction rate [14]; the activation process was shown to control the rate and mechanism of coating deposition [16], while substrate morphology affects the roughness, hydrophobicity, and thermal conductivity of the electroless coating [17]. The composition and annealing treatment were shown to affect the continuity of the coatings [18].

On the other hand, the electrodeposition process (ELD) is an easy and cost-effective method to fabricate nanostructures of various materials including metal and semiconductor oxide with tailored composition, thickness, and morphology by simply adjusting the electrochemical parameters [9,19]. ELD process can be carried out at low temperature in atmospheric conditions and requires a simple and cheap setup [20]. The ELD technique has showed high potential to be used in the nanophotonics, specifically in optoelectronic industry [9], photovoltaics, and superconductor applications as it allows the fabrication of large uniform areas of tailored films at low cost [21] and high crystallinity [22].

In the photovoltaics field, some amorphous silicon [23], CuInGaSe₂ [24] or Cu₂ZnSn(S,Se)₄ [25] solar cells were reported as BIPV. The semiconductor heterojunction solar cells (SCs) attracted increased interest because of the advantages such as high efficiency [26], easy fabrication, and low cost [27]. Among the different heterojunction solar cells such as intrinsic thin-layer, silicon, CdTe/CdS, CIGS/CdS [28], it was indicated that the ZnO/Cu₂O [29,30] ones show a great absorption in the UV-visible region [31], their components being non-toxic and earth-abundant [32]. Furthermore, the alignment of ZnO/Cu₂O heterojunction allows the separation and transportation of electro-hole pairs [33,34]. The ZnO/Cu₂O heterojunction SCs can be fabricated by techniques including thermal oxidation, plasma evaporation, sputtering, chemical vapor deposition, pulsed laser deposition, and electrodeposition [35–37]. The electrodeposition approach is easy, low cost, and scalable [35,36] which makes it highly appropriate.

The ZnO/Cu₂O heterojunctions are usually fabricated onto glass substrates coated with transparent conductive oxides (TCOs) such as indium-doped tin oxide (ITO) [38–42] or fluorine-doped tin oxide (FTO) [43–45] playing the role of frontal contact [46]. Such TCOs are employed because of their high transparency and conductivity that reduce the resistive losses [47]. These TCOs are used in the amorphous silicon solar cells as they allow the improvement in the solar light management [48]. Nevertheless, their high cost and chemical instability triggered researches toward reducing their use [48,49]. One of the alternatives to TCOs is an electroless coating which could also extend the application toward an insulating substrate such as a ceramic tile, polymers, or biomaterials [50,51]. Among the electroless coatings, the Ni-Mo-P one was reported for the fabrication of varying devices such as supercapacitor electrode [52] and proton exchange membrane fuel cells [53]. It is thus, of great challenge to find cheap insulating supports while employing scalable and low cost electrical functionalization and deposition, respectively, for optoelectronic devices [54].

The novelty of this study relies on the use of a ceramic tile as substrate for the fabrication of ZnO/Cu₂O heterojunction solar cells. To this end, the ceramic surface was subjected to electroless deposition of a Ni-Mo-P coating to be further employed as electrode for the synthesis of the ZnO and Cu₂O films by electrochemical deposition. The Ni-Mo-P coating was selected because of its easy fabrication and good electrical properties. It is known that electrodeposited material properties are directly dependent on the substrate properties. Therefore, in order to understand the effects of electroless plating on the fabrication and performance of electrodeposited heterojunctions, the electroless deposition duration and heat treatment in vacuum conditions on the Ni-Mo-P properties are studied along with the electrodeposition parameters such as potential and duration in order to tailor the properties of the heterojunction toward improved performance in photovoltaics.

2. Materials and Methods

2.1. Materials and Reagents

All chemicals were reagent grade and were used as received (Panreac, Barcelona, Spain). Palladium catalyst was prepared as reported elsewhere [8]. Ceramic substrate was fabricated from commercial powder (Euroatomizado, Valencia, Spain) as reported elsewhere [8].

2.2. Electroless Plating of the Ceramic Surface

First, the ceramic surface was activated with palladium catalyst at 300 °C for 12 h [8]. Then, the electroless plating of Ni-Mo-P film was performed at 80 °C and 300 rpm stirring rate from a bath composed of: NiSO₄, Na₂MoO₄, NaH₂PO₂, C₆H₁₂O₇, and Na₂C₄H₄O₆ in concentration (g L⁻¹) of 7, 3.9, 10.0, 15.0, and 10, respectively. NH₄OH was used to adjust the pH to 10. The metallized ceramic was further rinsed with water and air-dried. The plating time was varied from 30 to 300 min while the annealing treatment in vacuum conditions ranged from 160 °C for 16 h to 400 °C for 1 h (the metallized ceramic substrates were denoted as CS_{x-y} where *x* is the plating time and *y* is the applied heat treatment). These substrates were used to fabricate the p–n heterojunction solar cells.

2.3. Electrodeposition of ZnO on Ni-Mo-P/Ceramic Substrate

In order to fabricate the p–n heterojunction SCs using metallized ceramic substrates, electrodeposition (ELD) technique was selected. ZnO was electrodeposited onto Ni-Mo-P-coated ceramic substrates from 5 mM ZnCl₂ and 0.1 M KCl [29] in a deposition potential ranging from –0.6 to –0.8 V for 30 and 60 min at 75 °C in order to analyze the growth of ZnO layer and its effect on the performance of heterojunction SC using different substrates. In order to reference the electrodeposition of ZnO to the literature, a different batch of ceramic electrodes were obtained by coating the ceramic with an ITO layer with an electrical conductivity of about 1.8 μΩ cm and thickness of 300 nm.

2.4. Fabrication of Cu₂O/ZnO Heterojunction Solar Cells on Ni-Mo-P/Ceramic Substrate

Following the electrodeposition of ZnO layer, a Cu₂O layer was electrodeposited at 35 °C, –0.6 V for 300 min from an electrolyte composed of 0.4 M CuSO₄, 3 M C₃H₆O₃, and 4 M NaOH [55]. The final device was sealed with conductive carbon cement (Leit-C, Agar Scientific, Essex, UK) at the Cu₂O side [29,30].

2.5. Methods

All the electrochemical measurements were performed using a conventional three-electrode glass cell and potentiostat (PGSTAT 101 AUTOLAB, Metrohm, Madrid, Spain). The working electrode was the modified ceramic substrate while a Pt foil and an Ag/AgCl in saturated KCl electrode served as counter-electrode and reference electrode, respectively.

The deposition of ITO layer as reference electrode was achieved by DC magnetron sputtering (K675X, Emitech, Fall River, MA, USA) technique in Ar atmosphere, by using an In₂O₃/SnO₂ 90/10 wt % target (Kurt J. Lesker, East Sussex, UK). An annealing treatment was further performed in a tubular oven (Carbolite) at 260 °C for 30 min in N₂ with 4% H₂ atmosphere.

The structural properties of the electroless coating and ZnO/Cu₂O heterojunction synthesized onto ceramic substrates were investigated by X-ray diffraction (XRD) using an Ultima IV diffractometer (Rigaku, Barcelona, Spain) in the Bragg–Brentano configuration with CuKα radiation (1.54 Å). Atomic force microscopy (AFM, Multimode 8, Bruker, Madrid, Spain) and field emission scanning electron microscopy (FESEM, Bruker, Madrid, Spain working voltage 2 kV) techniques were used to determine the roughness and morphology of coatings. The electrical resistivity of coatings was determined by a four-point probe. The electrical properties of the solar cells were analyzed with a Sun 2000 Solar

Simulator (ABET Technologies, Madrid, Spain) working with $800 \text{ W}\cdot\text{m}^{-2}$ irradiation on the ZnO window in agreement to the scheme in Figure 1 [45,56,57].

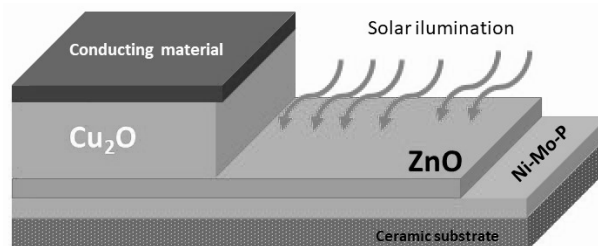


Figure 1. Schematic of limitation of p–n heterojunction solar cells onto electroless coated ceramic.

3. Results and Discussion

3.1. Electrodeposition Study

The first approach in the study of ZnO electrodeposition onto the ceramic substrate considered an ITO coating onto the ceramic surface in order to have a reference point of view on ZnO electrodeposition with respect to the literature. The ZnO electrodeposition onto ITO/ceramic substrate was performed by potentiostatic mode at the deposition potential $-0.8 \text{ V vs. Ag/AgCl}$, as indicated by previous studies [29]. The related chronoamperogram is further presented in Figure 2A. The evolution of the process is found to agree with reported results, and the nucleation process is reached in about 100 s (see inset) [58] while the current plateau value establishes at about 0.75 mA cm^{-2} . These results indicate that the properties of ITO coating onto the ceramic surface allow the nucleation and growth of ZnO structure by offering the necessary nucleation centers. Therefore, the ceramic substrate could be successfully employed as support for the fabrication of ZnO/Cu₂O heterojunction upon coating with a conductive layer.

Further, Ni-Mo-P coating was deposited onto the ceramic surface in order to be employed as substrate for the electrodeposition of ZnO films. Given that morphology and electrical properties of the substrate affect the nucleation and growth of an electrodeposited film [59], the effect of plating duration and annealing treatment of Ni-Mo-P coating onto the ZnO electrodeposition were studied as shown in Figure 2B–D. First, a cathodic linear sweep was performed in order to investigate the deposition process of ZnO—see Figure 2B. It can be observed that the reduction current increases above -0.4 V and a peak is formed at about -0.6 V which is attributed to the reduction process and formation of ZnO layer. The reduction peak is followed by a steady increase in the cathodic current and a steep increase in current above -1 V which is attributed to the deposition of Zn metal [60]. Therefore, it is indicated that the optimum electrodeposition potential of ZnO onto Ni-Mo-P coating ranges from -0.6 V to $-0.8 \text{ V vs. Ag/AgCl}$. The other conditions for deposition of the Ni-Mo-P coating resulted in similar evolution of deposition potential for ZnO, however differences in the current response were recorded as described further.

The increase in Ni-Mo-P electroless deposition duration (30 to 300 min) was observed to induce a decrease in electrical resistivity from $10.6 \mu\Omega\cdot\text{cm}$ to $0.843 \mu\Omega\cdot\text{cm}$ [61]. Consequently, the cathodic current plateau value for ZnO electrodeposition at -0.8 V on corresponding substrates (see Figure 2C) increased because of an improved morphology and more active sites created at the surface of the Ni-Mo-P coating [62].

On the other hand, an annealing treatment was indicated to improve the coating conductivity [63]. In this study, the electrical resistivity of the electroless coating obtained at 300 min further decreased upon annealing treatment at $160 \text{ }^\circ\text{C}$ for 16 h, reaching a value of $0.210 \Omega\cdot\text{sq}^{-1}$. The ZnO nucleation and growth process were observed to be better defined on the annealed Ni-Mo-P coating and as such, the current plateau increased [63]. It is evident that the nucleation is faster in the case of annealed

Ni-Mo-P coating (about 250 s), while the current plateau is more stable, as well, and it indicates a more homogeneous growth of ZnO.

Furthermore, the electrodeposition of ZnO was studied with the deposition potential at the surface of Ni-Mo-P coated ceramic that performed best, namely the one coated with Ni-Mo-P film deposited for 300 min and annealed at 160 °C for 16 h. Figure 2D shows the current transients corresponding to the formation of ZnO onto such substrates. As it can be seen, the current plateau increases with the applied potential, which is in agreement with literature, indicating an improved deposition rate at an overpotential value [64]. The nucleation process was observed to take place faster and change from a progressive trend toward an instantaneous one with the increase in the deposition potential.

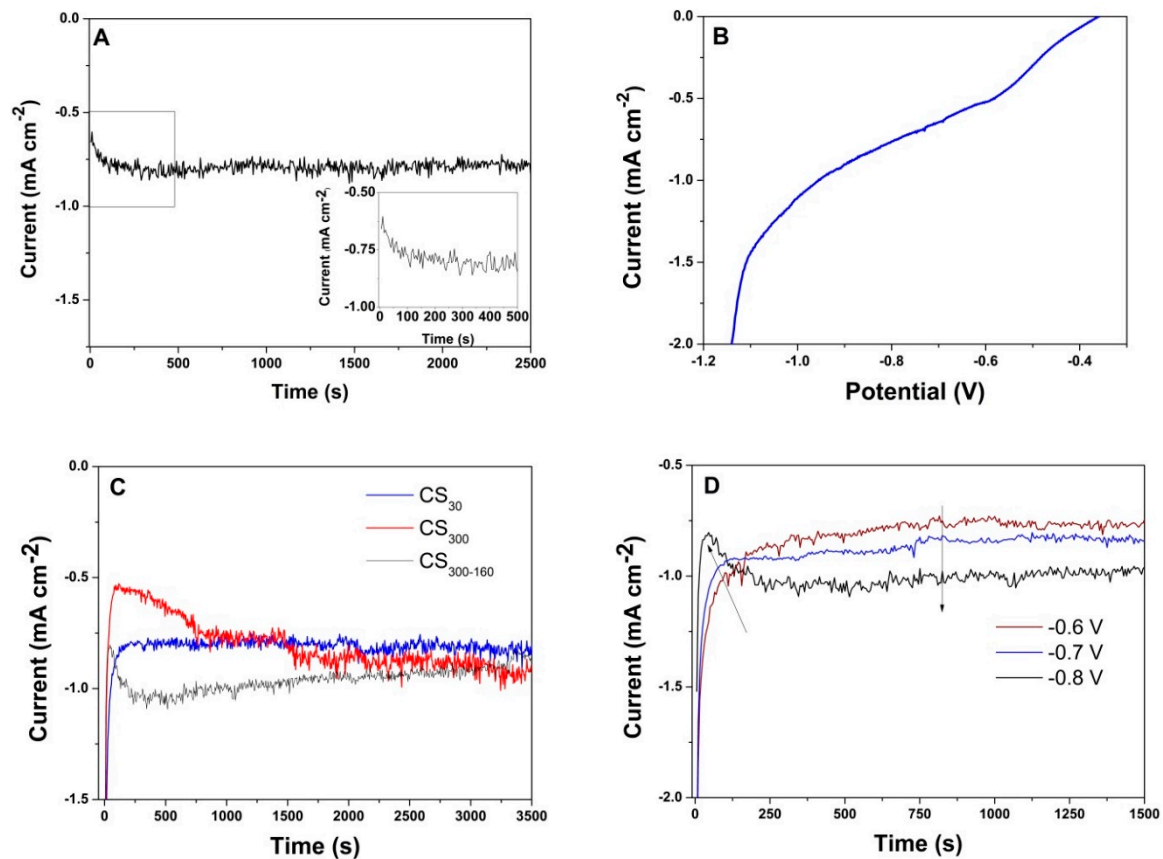


Figure 2. (A) Current transients for the electrodeposition of ZnO onto indium-doped tin oxide (ITO)/ceramic substrate (CS_{ITO}) and inset: magnified area of initial transients; (B) linear scan voltammetry of ZnO onto metallized ceramic substrates CS_{30} ; (C) current transients for the electrodeposition of ZnO on Ni-Mo-P/ceramic substrate as function of coating conditions (metallized ceramic substrates— CS_{x-y} , where x duration (minutes) of annealing and y —temperature of annealing (°C)); (D) current transients for the electrodeposition of ZnO on Ni-Mo-P/ceramic substrate ($CS_{300-160}$) with applied potential.

3.2. Morphology Analysis

Beside the electrical properties, the substrate roughness is also known to highly affect the properties of an electrodeposited film [65]. Therefore, morphology analysis was performed on the coated substrates by AFM technique. Figure 3 presents the AFM micrographs of the ceramic substrates upon coating with ITO and Ni-Mo-P films in terms of amplitude and topography. Initially, the bare ceramic substrate was found to exhibit a roughness value (Rq) of 412 ± 40 nm (not shown). Upon coating with ITO the ceramic surface showed a slight decrease in the roughness down to 396.8 ± 20 nm [48]—see Figure 3a,b.

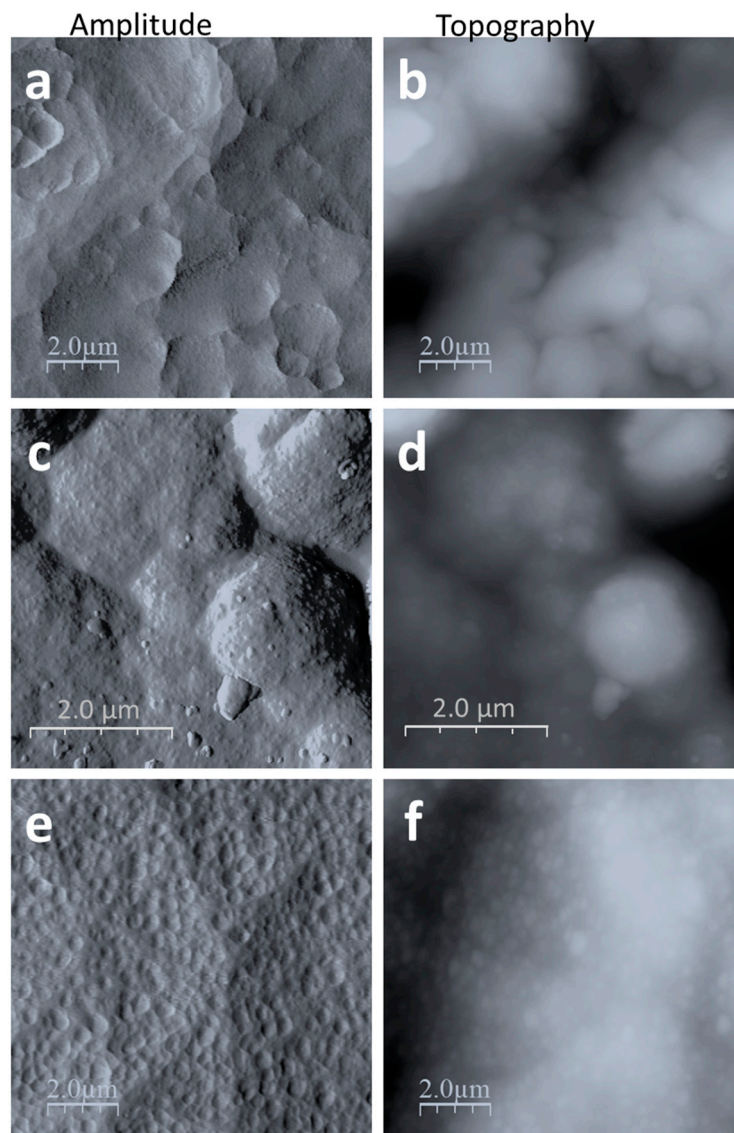


Figure 3. AFM micrographs (amplitude and topography) of ceramic substrate coated with ITO (a,b) and Ni-Mo-P coating without annealing at 30 min (c,d) and 300 min (e,f).

Figure 3c–f shows the appearance of the Ni-Mo-P coatings obtained with a palladium activation process at 300 °C for 12 h and autocatalytic chemical reduction at 80 °C for 30 and 300 min, respectively. Under these conditions, the coatings show an increment of roughness from ~76 to ~223 nm, attributed to the increase of the electroless deposition duration. Nevertheless, the AFM micrographs show the Ni-Mo-P coatings are homogeneous.

Figure 4 shows the effect of annealing on the Ni-Mo-P coating properties by depicting the FE-SEM micrographs of the ceramic substrates with a Ni-Mo-P coating in different conditions. As observed in Figure 4a, Ni-Mo-P coating annealed at low temperature as 160 °C for 16 h shows uniform, continuous, and compact nodular morphology. In order to obtain a smoother coating, the annealing temperature was increased to 400 °C, however a network of cracks breaking the continuous structure of the layer was observed (Figure 4b). This defect may be due to the increase in the crystallization degree with temperature [66] or thermal expansion coefficient mismatch between coating and substrate. For such a temperature value, only 1 h of annealing was studied, given the detrimental effects on the continuity of the coating. In this context, other authors indicate that the application of a thermal treatment with a temperature higher than 350 °C can negatively affect the morphology and topography of the surface of the coating [67,68]. The annealing treatment slightly reduced the surface resistivity from $0.210 \Omega \cdot \text{sq}^{-1}$

(coating annealed at 160 °C for 16 h) to $0.185 \Omega \cdot \text{sq}^{-1}$ (coating annealed at 400 °C for 1 h) being attributed to improved crystallinity [63].

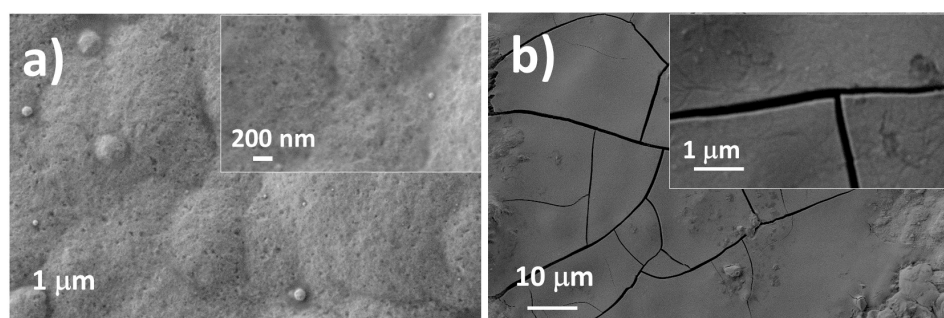


Figure 4. FE-SEM micrographs of Ni-Mo-P coating obtained by electroless process: (a) at 300 min under vacuum annealing at 160 °C for 16 h with inset: the SEM image of the coating at higher magnification and (b) at 400 °C for 1 h with inset: the SEM image of the coating at higher magnification.

The evolution of roughness and morphology of the Ni-Mo-P coating with plating duration and annealing treatment is in high agreement with the electrochemical results on ZnO growth. It is known that the density and growth orientation of ZnO nanostructures further affect the morphology properties of Cu_2O . Figure 5 depicts the effect of ZnO electrodeposited at -0.8 V on the morphology of Cu_2O films by SEM. While the presence of ZnO structures is not appreciated in the images, a good Cu_2O coverage is observed which is indicative of good interaction and crystallographic quality of the $\text{Cu}_2\text{O}/\text{ZnO}$ interface [69,70]. The morphology of the Cu_2O layer is markedly influenced by ZnO electrodeposition time, namely with an increase in electrodeposition duration from 30 min to 60 min, cubic structures of Cu_2O with a larger grain size are obtained, which is indicative of a thicker layer of Cu_2O (Figure 5b) and it is expected to improve the light absorption because of the fact that there are fewer grain edges [70].

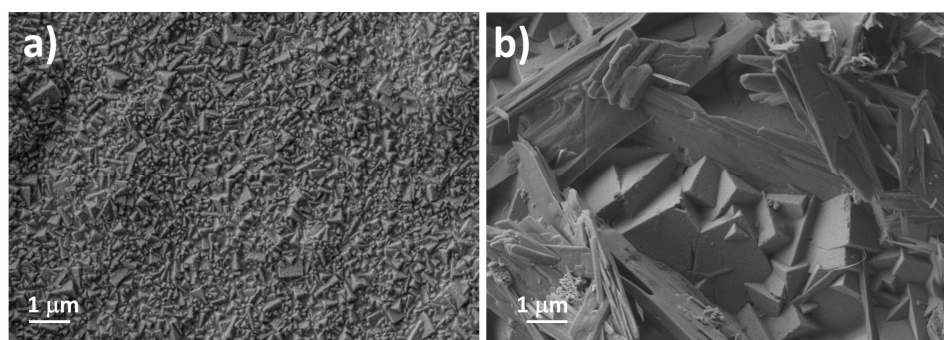


Figure 5. FE-SEM micrographs of Cu_2O electrodeposited onto ZnO layer obtained at -0.8 V for 30 min (a) and 60 min (b).

3.3. Structure Analysis

The structure and orientation of the electrodeposited heterojunctions were further analyzed by XRD measurements. First, the diffraction patterns of Ni-Mo-P coating obtained for varying duration are depicted in Figure 6A. The results indicate the metallic Ni-Mo-P coatings present a Ni crystalline structure because of the presence of the reflection peaks of Ni (111), corresponding to the cubic phase centered on the face of Ni [71] and Ni (200) which appear around 44° and 51.3° [72]. Furthermore, the increase in the duration of electroless plating results in an increase in crystallite size which is evidenced in the reduction in full width of half maximum (FWHM) of the predominant peak [73].

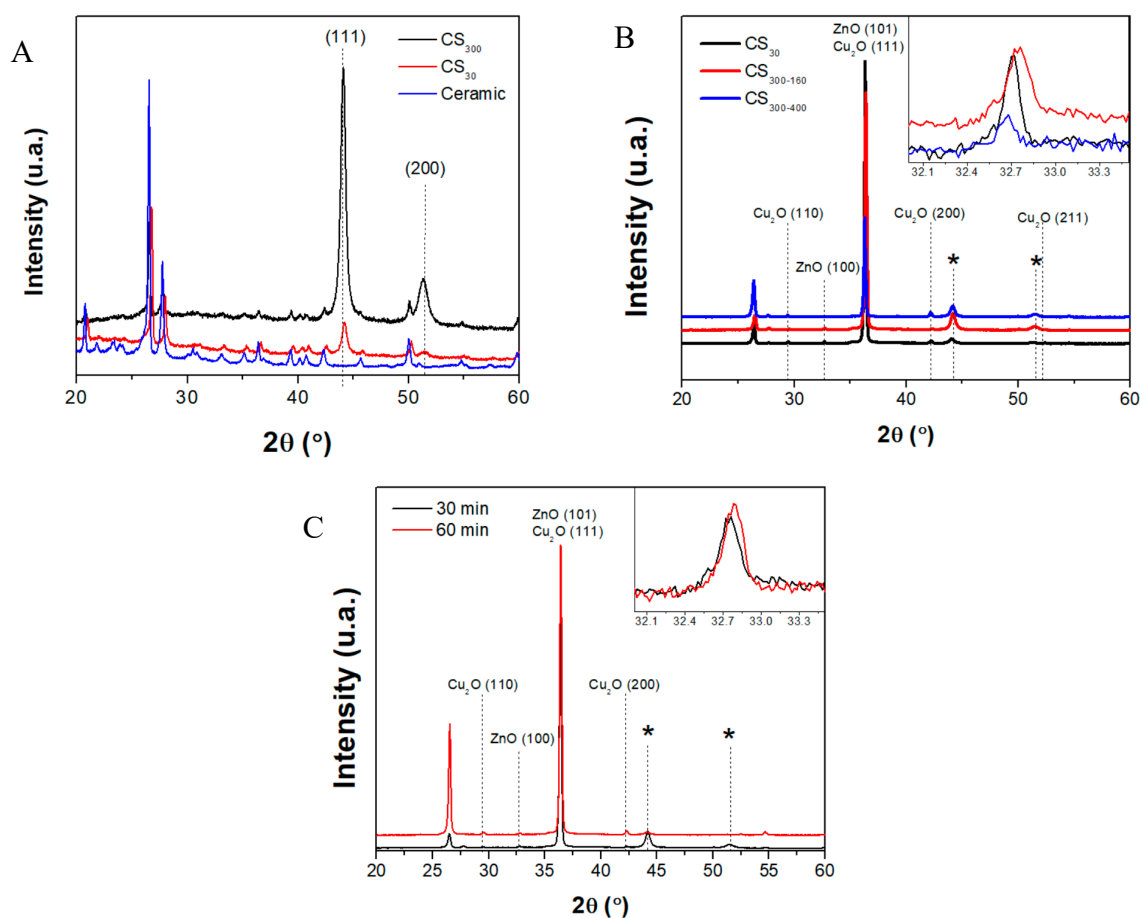


Figure 6. X-ray diffraction patterns of ceramic substrate: (A) before and after plating with Ni-Mo-P for 30 and 300 min; (B) Cu₂O/ZnO heterojunctions onto different Ni-Mo-P coating (*) with inset representing the ZnO (100) peak; (C) Cu₂O/ZnO heterojunctions onto Ni-Mo-P coating CS₃₀₀₋₁₆₀ (*) with ZnO deposition duration with inset presenting the ZnO (100).

The corresponding XRD diffraction patterns of the Cu₂O/ZnO heterojunctions electrodeposited on Ni-Mo-P films plated for varying duration with or without annealing are further shown in Figure 6B. Ni-Mo-P coating peaks (labeled with *) appear at 44° and 52°, the other peaks are typical of the ceramic substrate. The presence of ZnO layer is clearly evidenced in agreement with the JCPDS identification card 00-036-1451 [43], corresponding to a wurtzite-type hexagonal crystalline structure with a (101) preferential orientation which was attributed to branched ZnO nanowires [74] as an effect of applied temperature [75]. This peak is overlapped with a Cu₂O one, namely (111), in agreement with other reports [76]. The analysis of the characteristic peak ZnO (100) (inset) indicates the crystallite size decreases upon growing the ZnO layer onto a Ni-Mo-P coating annealed at 160 °C, which suggests a greater number of p–n junctions with Cu₂O. However, when applying a higher temperature annealing treatment (400 °C for 1 h) to the Ni-Mo-P substrate, the ZnO (100) peak is shifted probably because of stress in the crystal lattice. On the other hand, cubic structure of Cu₂O layer was identified by the presence of planes (110), (111), (200), and (211) (JCPDS card 00-005-0667) [45].

The effect of the electroplating time of the ZnO layer was further investigated. Ni-Mo-P coating annealed at 160 °C for 16 h was employed as substrate, as it exhibited the best performance for ED. The corresponding diffractograms of the Cu₂O/ZnO heterojunctions are shown in Figure 6C. The diffraction patterns are similar to the previous one, with wurtzite hexagonal crystalline structure and a preferential orientation in the plane (101) for the ZnO layer. The characteristic peak ZnO (100) (see inset) slightly changed in terms of FWHM and position which is indicative of smaller crystallite size [77] with the increase in the electrodeposition time to 60 min, which suggests an improved density

of heterojunctions [29,78,79]. Regarding the synthesized Cu_2O layers, they showed similar pattern as previously shown with the previous samples.

3.4. Photoelectrical Properties of $\text{Cu}_2\text{O}/\text{ZnO}$ Heterojunction Solar Cells Supported onto Ni-Mo-P-Coated Ceramic

The short circuit current density (J_{SC}) and open circuit voltage (V_{OC}) photoelectric parameters obtained for varying $\text{Cu}_2\text{O}/\text{ZnO}$ heterojunction solar cells supported onto Ni-Mo-P coated ceramic are shown in Table 1. It was observed that all the $\text{Cu}_2\text{O}/\text{ZnO}$ heterojunction solar cells show photoelectric properties, however, the $\text{Cu}_2\text{O}/\text{ZnO}$ heterojunction solar cell fabricated onto ITO coating exhibited the lowest J_{SC} values which could be explained by the properties of the ITO layer that need optimizing.

Table 1. Photoelectric parameters of $\text{Cu}_2\text{O}/\text{ZnO}$ heterojunction solar cells (SCs) with Ni-Mo-P plating conditions.

Solar Cell	J_{SC} ($\mu\text{A}/\text{cm}^2$)	V_{OC} (μV)
$\text{Cu}_2\text{O}/\text{ZnO}/\text{CS}_{\text{ITO}}$	1.51	544.032
$\text{Cu}_2\text{O}/\text{ZnO}/\text{CS}_{30}$	39.92	383.229
$\text{Cu}_2\text{O}/\text{ZnO}/\text{CS}_{300}$	27.25	532.648
$\text{Cu}_2\text{O}/\text{ZnO}/\text{CS}_{300-160}$	939.96	454.338
$\text{Cu}_2\text{O}/\text{ZnO}/\text{CS}_{300-400}$	4.64	620.602

The photoelectric properties of the heterojunction SC induced by Ni-Mo-P plating conditions were analyzed. Thus, by increasing the plating duration for Ni-Mo-P film from 30 to 300 min, the heterojunction SC exhibited improved V_{OC} value while the J_{SC} values slightly decreased. This improvement is mainly attributed to the improved homogeneity and low resistivity of the electroless Ni-Mo-P coating. Upon annealing at 160 °C for 16 h of the Ni-Mo-P plated for 300 min, a significant improvement in the photoelectric properties is observed, that is the J_{SC} markedly increased while the V_{OC} slightly decreased, which could be explained by improved properties of ZnO layer derived from smaller lattice mismatch of the Ni-Mo-P coating and the ZnO layer as well as the reduction in resistivity of Ni-Mo-P. Clearly, an annealing temperature as high as 400 °C for the Ni-Mo-P coating negatively affects the photoelectric properties of the heterojunction SC as J_{SC} markedly drops. This decrease may be due to the cracks in the coating as indicated by microscopy results that causes short circuits reducing the SC performance [80]. Such results show the optimum conditions among the parameters studied for Ni-Mo-P plating, which are duration of 300 min and the application of an annealing treatment at 160 °C for 16 h.

The photoelectric properties of the heterojunction SC supported on Ni-Mo-P-coated ceramic (electroless plating 300 min with heat treatment at 160 °C for 16 h) as induced by ZnO electrodeposition conditions were further investigated and presented in Table 2.

Table 2. Effect of electrodeposition process (ELD) conditions for ZnO on the photoelectric parameters of $\text{Cu}_2\text{O}/\text{ZnO}$ heterojunction SCs supported on Ni-Mo-P-coated ceramic.

ELD Condition of ZnO	J_{SC} ($\mu\text{A}/\text{cm}^2$)	V_{OC} (μV)
−0.6 V; 30 min	52.48	713.53
−0.7 V; 30 min	719.75	659.27
−0.8 V; 30 min	939.96	454.34
−0.8 V; 60 min	1440	760.23

It was observed that increasing the electrodeposition potential of ZnO layer markedly improves the J_{SC} value of the SC while V_{OC} decreases, which indicates good crystallinity of the ZnO layer. By further increasing the deposition duration, the J_{SC} value reached 1.44 $\text{mA}\cdot\text{cm}^{-2}$ and V_{OC} improved. This improvement in the photoelectric properties (J_{SC}) may be due to the good interconnection and

crystallographic quality of the Cu₂O/ZnO interface and improved properties of ZnO nanostructures such as density and aspect ratio that could improve charge transport [69]. The increase in V_{OC} value is an indication of reduced grain limits and improved light absorption [70].

4. Conclusions

A ZnO/Cu₂O heterojunction type solar cell was fabricated onto ceramic substrate by simple electrodeposition technique. The electrical functionalization of the ceramic surface has been achieved by electroless coating of a Ni-Mo-P film. Continuous and homogeneous Ni-Mo-P coatings were obtained with typical XRD reflection planes. The results indicated the morphology and electrical conductivity of Ni-Mo-P film can be easily tailored by adjusting the electroless coating conditions such as duration and by applying an appropriate annealing treatment, namely lower temperature for long time. The increase in applied potential and duration for ZnO electrodeposition, namely -0.8 V for 1 h resulted in the best performance of the ZnO/Cu₂O heterojunction type solar cell, that is, $1.44 \text{ mA}\cdot\text{cm}^{-2}$ for the J_{SC} and $760.23 \text{ }\mu\text{V}$ for the V_{OC} value, respectively, which demonstrates the importance of electrodeposition of ZnO layer toward improving the photoelectrical parameters of the heterojunction solar cell. Although the performance still need improvements of the photoelectric parameters, the obtained results show that an insulating substrate (in this case a ceramic tile) could be used for electrical power generation applications by applying a Ni-Mo-P electroless coating. The results of this work indicate that optimized electrochemical growth of the heterojunction layers, annealing treatment, and the tailoring of the ZnO/Cu₂O interface are parameters of paramount importance for solar cell performance improvement.

Author Contributions: Conceptualization, N.M.R.-L., A.I.P., J.C.; methodology, N.M.R.-L. and A.I.P.; investigation, N.M.R.-L., A.I.P., J.C., and D.B.-M.; data curation, N.M.R.-L. and A.I.P.; writing—original draft preparation, N.M.R.-L.; writing—review and editing, N.M.R.-L., A.I.P., J.C., and D.B.-M. All authors have read and agreed to the published version of the manuscript.

Funding: This research received no external funding.

Acknowledgments: The technical support from Servicio de Microscopía Electrónica, UPV and Instituto Universitario de Tecnología Nanofotónica, UPV is highly acknowledged.

Conflicts of Interest: The authors declare no conflict of interest.

References

1. Kishawy, H.A.; Hosseini, A. *Machining Difficult-to-Cut Materials*; Materials Forming, Machining and Tribology; Springer International Publishing: Cham, Switzerland, 2019; ISBN 978-3-319-95965-8.
2. Leali, P.T.; Merolli, A. Fundamentals of Biomaterials. In *Biomaterials in Hand Surgery*; Springer Milan: Milano, Italy, 2009; pp. 1–11. ISBN 9788847011946.
3. Ghosh, S.; Pal, K.S.; Dandapat, N.; Datta, S.; Basu, D. Interfacial properties of metallized alumina ceramics. *Met. Mater. Int.* **2012**, *18*, 625–630. [[CrossRef](#)]
4. Ene Hourdequin, H.; Laudebat, L.; Locatelli, M.-L.; Valdez-Nava, Z.; Bidan, P. Metallized ceramic substrate with mesa structure for voltage ramp-up of power modules. *Eur. Phys. J. Appl. Phys.* **2019**, *87*, 20903. [[CrossRef](#)]
5. Mirone, G.; Sitta, A.; D'Arrigo, G.; Calabretta, M. Material Characterization and Warpage Modeling for Power Devices Active Metal Brazed Substrates. *IEEE Trans. Device Mater. Reliab.* **2019**, *19*, 537–542. [[CrossRef](#)]
6. Sampaio, P.G.V.; Gonzi, M.O.A. Photovoltaic solar energy: Conceptual framework. *Renew. Sustain. Energy Rev.* **2017**, *74*, 590–601. [[CrossRef](#)]
7. Agarwala, R.C.; Agarwala, V. Electroless alloy/composite coatings: A review. *Sadhana* **2003**, *28*, 475–493. [[CrossRef](#)]
8. Rosas-Laverde, N.M.; Pruna, A.; Cembrero, J.; Pascual, M.; Orozco-Messana, J. Optimizing Electroless Plating of Ni–Mo–P Coatings Toward Functional Ceramics. *Acta Metall. Sin. Engl. Lett.* **2020**, *33*, 1–9. [[CrossRef](#)]

9. Badán, J.A.; Navarrete-Astorga, E.; Henríquez, R.; Martín, F.; Marotti, R.E.; Ramos-Barrado, J.R.; Dalchiele, E.A. Optical properties of silver nanoparticles deposited onto silicon substrates by different soft-solution processing techniques. *Opt. Mater. (Amst)* **2020**, *100*, 109651. [[CrossRef](#)]
10. Ma, H.; Liu, Z.; Wu, L.; Wang, Y.; Wang, X. Study of a pre-treatment process for electroless copper plating on ceramics. *Thin Solid Films* **2011**, *519*, 7860–7863. [[CrossRef](#)]
11. Zhang, B. Electroless Plating Baths of Metals, Binary Alloys, and Multicomponent Alloys. In *Amorphous and Nano Alloys Electroless Depositions: Technology, Composition. Structure and Theory*; Tian, S., Ed.; Elsevier: Amsterdam, The Netherlands, 2016; pp. 51–106. ISBN 9780128026854.
12. Zhang, B. Impact Parameters and Deposition Rate. In *Amorphous and Nano Alloys Electroless Depositions: Technology, Composition. Structure and Theory*; Tian, S., Ed.; Elsevier: Amsterdam, The Netherlands, 2016; pp. 323–381. ISBN 9780128026854.
13. Heidarzadeh, A.; Mousavian, R.T.; Khosroshahi, R.A.; Afkham, Y.A.; Pouraliakbar, H. Empirical model to predict mass gain of cobalt electroless deposition on ceramic particles using response surface methodology. *Rare Met.* **2017**, *36*, 209–219. [[CrossRef](#)]
14. Zhou, R.; Chen, H.; Xu, C.; Hou, X.; Liu, G.; Liu, Y. Facile synthesis of electromagnetic Ni@glass fiber composites via electroless deposition method. *J. Mater. Sci. Mater. Electron.* **2015**, *26*, 3530–3537. [[CrossRef](#)]
15. Tai, Y.; Chen, H.; Xu, C.; Liu, Y. Conductive glass fabrics@nickel composites prepared by a facile electroless deposition method. *Mater. Lett.* **2016**, *171*, 158–161. [[CrossRef](#)]
16. Lee, C.-L.; Wan, C.-C.; Wang, Y.-Y. Pd Nanoparticles as a New Activator for Electroless Copper Deposition. *J. Electrochem. Soc.* **2003**, *150*, C125. [[CrossRef](#)]
17. Lin, J.D.; Kuo, C.L. Effects of hydrogen plasma treatment on microstructure evolution and electrical conductivity of electroless Ni-P coatings on polyimide and glass substrates. *Surf. Coatings Technol.* **2012**, *209*, 80–89. [[CrossRef](#)]
18. Kazemi, A.; Yang, S. Atomistic Study of the Effect of Magnesium Dopants on the Strength of Nanocrystalline Aluminum. *JOM* **2019**, *71*, 1209–1214. [[CrossRef](#)]
19. Li, Q.; Xu, M.; Fan, H.; Wang, H.; Peng, B.; Long, C.; Zhai, Y. Dielectric properties investigation of Cu₂O/ZnO heterojunction thin films by electrodeposition. *Mater. Sci. Eng. B Solid-State Mater. Adv. Technol.* **2013**, *178*, 496–501. [[CrossRef](#)]
20. Li, J.; Li, H.; Xue, Y.; Fang, H.; Wang, W. Facile electrodeposition of environment-friendly Cu₂O/ZnO heterojunction for robust photoelectrochemical biosensing. *Sensors Actuators B Chem.* **2014**, *191*, 619–624. [[CrossRef](#)]
21. Bhattacharya, R.N.; Deb, S.K. A Low-Cost Approach to Fabrication of Multinary Compounds for Energy-Related Applications. *Jpn. J. Appl. Phys.* **2000**, *39*, 424. [[CrossRef](#)]
22. Kang, D.; Lee, D.; Choi, K.-S. Electrochemical Synthesis of Highly Oriented, Transparent, and Pinhole-Free ZnO and Al-Doped ZnO Films and Their Use in Heterojunction Solar Cells. *Langmuir* **2016**, *32*, 10459–10466. [[CrossRef](#)]
23. Shah, A.V.; Schade, H.; Vanecek, M.; Meier, J.; Vallat-Sauvain, E.; Wyrsh, N.; Kroll, U.; Droz, C.; Bailat, J. Thin-film silicon solar cell technology. *Prog. Photovoltaics Res. Appl.* **2004**, *12*, 113–142. [[CrossRef](#)]
24. Rosa, G.; Bosio, A.; Menossi, D.; Romeo, N. How the Starting Precursor Influences the Properties of Polycrystalline CuInGaSe₂ Thin Films Prepared by Sputtering and Selenization. *Energies* **2016**, *9*, 354. [[CrossRef](#)]
25. Calvet, I.; Barrachina, E.; Martí, R.; Fraga, D.; Stoyanova Lyubenova, T.; Carda, J.B. Development of photovoltaic ceramic tile based on CZTSSe absorber. *Mater. Lett.* **2015**, *161*, 636–639. [[CrossRef](#)]
26. Lin, S.; Li, X.X.; Pan, H.; Chen, H.; Li, X.X.; Li, Y.; Zhou, J. Numerical analysis of In_xGa_{1-x}N/SnS and Al_xGa_{1-x}N/SnS heterojunction solar cells. *Energy Convers. Manag.* **2016**, *119*, 361–367. [[CrossRef](#)]
27. Cheng, K.; Li, Q.; Meng, J.; Han, X.; Wu, Y.; Wang, S.; Qian, L.; Du, Z. Interface engineering for efficient charge collection in Cu₂O/ZnO heterojunction solar cells with ordered ZnO cavity-like nanopatterns. *Sol. Energy Mater. Sol. Cells* **2013**, *116*, 120–125. [[CrossRef](#)]
28. Reinders, A.; Verlinden, P.; Van Sark, W.; Freundlich, A. (Eds.) *Photovoltaic Solar Energy*; John Wiley & Sons, Ltd.: Chichester, UK, 2016; ISBN 9781118927496.
29. Rosas-Laverde, N.M.; Pruna, A.; Cembrero, J.; Orozco-Messana, J.; Manjón, F.J. Performance of graphene oxide-modified electrodeposited ZnO/Cu₂O heterojunction solar cells. *Boletín Soc. Española Cerámica Vidr.* **2019**, *58*, 263–273. [[CrossRef](#)]

30. Rosas-Laverde, N.M.; Pruna, A.; Busquets-Mataix, D.; Marí, B.; Cembrero, J.; Salas Vicente, F.; Orozco-Messana, J. Improving the properties of Cu₂O/ZnO heterojunction for photovoltaic application by graphene oxide. *Ceram. Int.* **2018**, *44*, 23045–23051. [[CrossRef](#)]
31. Wang, C.; Xu, J.; Shi, S.; Zhang, Y.; Gao, Y.; Liu, Z.; Zhang, X.; Li, L. Optimizing performance of Cu₂O/ZnO nanorods heterojunction based self-powered photodetector with ZnO seed layer. *J. Phys. Chem. Solids* **2017**, *103*, 218–223. [[CrossRef](#)]
32. Elfadill, N.G.; Hashim, M.R.; Chahrour, K.M.; Qaeed, M.A.; Bououdina, M. The influence of Cu₂O crystal structure on the Cu₂O/ZnO heterojunction photovoltaic performance. *Superlattices Microstruct.* **2015**, *85*, 908–917. [[CrossRef](#)]
33. Bai, Z.; Zhang, Y. Self-powered UV-visible photodetectors based on ZnO/Cu₂O nanowire/electrolyte heterojunctions. *J. Alloys Compd.* **2016**, *675*, 325–330. [[CrossRef](#)]
34. Bai, Z.; Liu, J.; Liu, F.; Zhang, Y. Enhanced photoresponse performance of self-powered UV-visible photodetectors based on ZnO/Cu₂O/electrolyte heterojunctions via graphene incorporation. *J. Alloys Compd.* **2017**, *726*, 803–809. [[CrossRef](#)]
35. Tran, M.H.; Cho, J.Y.; Sinha, S.; Gang, M.G.; Heo, J. Cu₂O/ZnO heterojunction thin-film solar cells: The effect of electrodeposition condition and thickness of Cu₂O. *Thin Solid Films* **2018**, *661*, 132–136. [[CrossRef](#)]
36. Messaoudi, O.; Makhoulouf, H.; Souissi, A.; Ben assaker, I.; Amiri, G.; Bardaoui, A.; Oueslati, M.; Bechelany, M.; Chtourou, R. Synthesis and characterization of ZnO/Cu₂O core-shell nanowires grown by two-step electrodeposition method. *Appl. Surf. Sci.* **2015**, *343*, 148–152. [[CrossRef](#)]
37. Jiang, X.; Lin, Q.; Zhang, M.; He, G.; Sun, Z. Microstructure, optical properties, and catalytic performance of Cu₂O-modified ZnO nanorods prepared by electrodeposition. *Nanoscale Res. Lett.* **2015**, *2–7*. [[CrossRef](#)] [[PubMed](#)]
38. Chen, J.W.; Perng, D.C.; Fang, J.F. Nano-structured Cu₂O solar cells fabricated on sparse ZnO nanorods. *Sol. Energy Mater. Sol. Cells* **2011**, *95*, 2471–2477. [[CrossRef](#)]
39. Panigrahi, S.; Nunes, D.; Calmeiro, T.; Kardarian, K.; Martins, R.; Fortunato, E. Oxide-Based Solar Cell: Impact of Layer Thicknesses on the Device Performance. *ACS Comb. Sci.* **2017**, *19*, 113–120. [[CrossRef](#)] [[PubMed](#)]
40. Jeong, S.; Aydil, E.S. Heteroepitaxial growth of Cu₂O thin film on ZnO by metal organic chemical vapor deposition. *J. Cryst. Growth* **2009**, *311*, 4188–4192. [[CrossRef](#)]
41. Kathalingam, A.; Vikraman, D.; Kim, H.S.; Park, H.J. Facile fabrication of n-ZnO nanorods/p-Cu₂O heterojunction and its photodiode property. *Opt. Mater. (Amst.)* **2017**, *66*, 122–130. [[CrossRef](#)]
42. Fujimoto, K.; Oku, T.; Akiyama, T.; Suzuki, A. Fabrication and characterization of copper oxide-zinc oxide solar cells prepared by electrodeposition. *J. Phys. Conf. Ser.* **2013**, *433*, 012024. [[CrossRef](#)]
43. Lahmar, H.; Setifi, F.; Azizi, A.; Schmerber, G.; Dinia, A. On the electrochemical synthesis and characterization of p-Cu₂O/n-ZnO heterojunction. *J. Alloys Compd.* **2017**, *718*, 36–45. [[CrossRef](#)]
44. Abdelfatah, M.; Ismail, W.; El-Shaer, A. Low cost inorganic white light emitting diode based on submicron ZnO rod arrays and electrodeposited Cu₂O thin film. *Mater. Sci. Semicond. Process.* **2018**, *81*, 44–47. [[CrossRef](#)]
45. Septina, W.; Ikeda, S.; Khan, M.A.; Hirai, T.; Harada, T.; Matsumura, M.; Peter, L.M. Potentiostatic electrodeposition of cuprous oxide thin films for photovoltaic applications. *Electrochim. Acta* **2011**, *56*, 4882–4888. [[CrossRef](#)]
46. Han, G.; Zhang, S.; Boix, P.P.; Wong, L.H.; Sun, L.; Lien, S.-Y. Towards high efficiency thin film solar cells. *Prog. Mater. Sci.* **2017**, *87*, 246–291. [[CrossRef](#)]
47. Barreau, N.; Duche, D.; Ruiz, C.M.; Escoubas, L.; Simon, J.-J.; Le Rouzo, J.; Bermudez, V. Innovative approaches in thin-film photovoltaic cells. In *Optical Thin Films and Coatings*; Elsevier: Amsterdam, The Netherlands, 2018; pp. 595–632.
48. Hamelmann, F.U. Transparent Conductive Oxides in Thin Film Photovoltaics. *J. Phys. Conf. Ser.* **2014**, *559*, 012016. [[CrossRef](#)]
49. Wu, S.; Yin, Z.; He, Q.; Huang, X.; Zhou, X.; Zhang, H. Electrochemical deposition of semiconductor oxides on reduced graphene oxide-based flexible, transparent, and conductive electrodes. *J. Phys. Chem. C* **2010**, *114*, 11816–11821. [[CrossRef](#)]

50. Arefpour, M.; Almasi Kashi, M.; Bagheli, M. High Chemical and Thermal Stability of Ag Nanowire-Based Transparent Conductive Electrodes Induced by Electroless Ag Nanoparticle Decoration. *Phys. status solidi* **2020**, *217*, 1900957. [[CrossRef](#)]
51. Jia, G.; Plentz, J.; Dellith, A.; Schmidt, C.; Dellith, J.; Schmidl, G.; Andrä, G. Biomimic Vein-Like Transparent Conducting Electrodes with Low Sheet Resistance and Metal Consumption. *Nano-Micro Lett.* **2020**, *12*, 1–13. [[CrossRef](#)]
52. Rosas-Laverde, N.M.; Pruna, A.I.; Busquets-Mataix, D. Graphene oxide-polypyrrole coating for functional ceramics. *Nanomaterials* **2020**, *10*, 1188. [[CrossRef](#)]
53. Fetohi, A.E.; Abdel Hameed, R.M.; El-Khatib, K.M. Ni-P and Ni-Mo-P modified aluminium alloy 6061 as bipolar plate material for proton exchange membrane fuel cells. *J. Power Sources* **2013**, *240*, 589–597. [[CrossRef](#)]
54. Nikoobakht, A.; Aghaei, J.; Massrur, H.R.; Hemmati, R. Decentralised hybrid robust/stochastic expansion planning in coordinated transmission and active distribution networks for hosting large-scale wind energy. *IET Gener. Transm. Distrib.* **2020**, *14*, 797–807. [[CrossRef](#)]
55. Cembrero-Coca, P.; Cembrero, J.; Busquets-Mataix, D.; Pérez-Puig, M.A.; Marí, B.; Pruna, A. Factorial electrochemical design for tailoring of morphological and optical properties of Cu₂O. *Mater. Sci. Technol. (UK)* **2017**, *33*, 2102–2109. [[CrossRef](#)]
56. Yang, M.; Zhu, L.; Li, Y.; Cao, L.; Guo, Y. Asymmetric interface band alignments of Cu₂O/ZnO and ZnO/Cu₂O heterojunctions. *J. Alloys Compd.* **2013**, *578*, 143–147. [[CrossRef](#)]
57. Pławecki, M.; Rówiński, E. Mieszczak Zinc oxide/cuprous(I) oxide-based solar cells prepared by electrodeposition. *Acta Phys. Pol. A* **2016**, *130*, 1144–1146. [[CrossRef](#)]
58. Rosas-Laverde, N.M.; Pruna, A.; Busquets-Mataix, D.; Pullini, D. Graphene oxide-assisted morphology and structure of electrodeposited ZnO nanostructures. *Materials (Basel)* **2020**, *13*, 365. [[CrossRef](#)] [[PubMed](#)]
59. Oliveira, F.F.; Proenca, M.P.; Araújo, J.P.; Ventura, J. Electrodeposition of ZnO thin films on conducting flexible substrates. *J. Mater. Sci.* **2016**, *51*, 5589–5597. [[CrossRef](#)]
60. Marimuthu, T.; Anandhan, N.; Thangamuthu, R. Electrochemical synthesis of one-dimensional ZnO nanostructures on ZnO seed layer for DSSC applications. *Appl. Surf. Sci.* **2018**, *428*, 385–394. [[CrossRef](#)]
61. Cui, X.; Hutt, D.A.; Conway, P.P. Evolution of microstructure and electrical conductivity of electroless copper deposits on a glass substrate. *Thin Solid Films* **2012**, *520*, 6095–6099. [[CrossRef](#)]
62. Sridhar, N.; Udaya Bhat, K. Effect of Deposition Time on the Morphological Features and Corrosion Resistance of Electroless Ni-High P Coatings on Aluminium. *J. Mater.* **2013**, *2013*, 985763. [[CrossRef](#)]
63. Liu, B.H.; Liao, F.Y.; Chen, J.H. Design, fabrication, and characterization of electroless Ni-P alloy films for micro heating devices. *Thin Solid Films* **2013**, *537*, 263–268. [[CrossRef](#)]
64. Pruna, A.; Shao, Q.; Kamruzzaman, M.; Li, Y.Y.; Zapien, J.A.; Pullini, D.; Busquets Mataix, D.; Ruotolo, A. Effect of ZnO core electrodeposition conditions on electrochemical and photocatalytic properties of polypyrrole-graphene oxide shelled nanoarrays. *Appl. Surf. Sci.* **2017**, *392*, 801–809. [[CrossRef](#)]
65. Prepelita, P.; Medianu, R.; Sbarcea, B.; Garoi, F.; Filipescu, M. The influence of using different substrates on the structural and optical characteristics of ZnO thin films. *Appl. Surf. Sci.* **2010**, *256*, 1807–1811. [[CrossRef](#)]
66. Mukhopadhyay, A.; Barman, T.K. Effect of heat treatment on tribological behavior of electroless Ni-B coating at elevated temperatures. *Surf. Rev. Lett.* **2018**, *25*, 1850014. [[CrossRef](#)]
67. Wang, S.; Zhang, W. Influence of heat treatment for coating of nickel plating on hollow glass beads. *Phys. Procedia* **2013**, *50*, 219–224. [[CrossRef](#)]
68. Makkar, P.; Agarwala, R.C.; Agarwala, V. Chemical synthesis of TiO₂ nanoparticles and their inclusion in Ni-P electroless coatings. *Ceram. Int.* **2013**, *39*, 9003–9008. [[CrossRef](#)]
69. Ke, N.H.; Trinh, L.T.T.; Phung, P.K.; Loan, P.T.K.; Tuan, D.A.; Truong, N.H.; Tran, C.V.; Hung, L.V.T. Changing the thickness of two layers: I-ZnO nanorods, p-Cu₂O and its influence on the carriers transport mechanism of the p-Cu₂O/i-ZnO nanorods/n-IGZO heterojunction. *SpringerPlus* **2016**, *5*, 710. [[CrossRef](#)] [[PubMed](#)]
70. Makhlof, H.; Weber, M.; Messaoudi, O.; Tingry, S.; Moret, M.; Briot, O.; Chtoutou, R.; Bechelany, M. Study of Cu₂O/ZnO nanowires heterojunction designed by combining electrodeposition and atomic layer deposition. *Appl. Surf. Sci.* **2017**, *426*, 301–306. [[CrossRef](#)]
71. Balaraju, J.N.; Raman, N.; Manikandanath, N.T. Nanocrystalline electroless nickel poly-alloy deposition: Incorporation of W and Mo. *Trans. IMF* **2014**, *92*, 169–176. [[CrossRef](#)]

72. Guo, Z.; Keong, K.G.G.; Sha, W. Crystallisation and phase transformation behaviour of electroless nickel phosphorus platings during continuous heating. *J. Alloys Compd.* **2003**, *358*, 112–119. [[CrossRef](#)]
73. Mukhopadhyay, A.; Barman, T.K.; Sahoo, P. Wear and friction characteristics of electroless Ni-B-W coatings at different operating temperatures. *Mater. Res. Express* **2018**, *5*, 26526. [[CrossRef](#)]
74. Lee, G.H. Relationship between crystal structure and photoluminescence properties of ZnO films formed by oxidation of metallic Zn. *Electron. Mater. Lett.* **2010**, *6*, 155–159. [[CrossRef](#)]
75. Lim, K.; Abdul Hamid, M.; Shamsudin, R.; Al-Hardan, N.H.; Mansor, I.; Chiu, W. Temperature-Driven Structural and Morphological Evolution of Zinc Oxide Nano-Coalesced Microstructures and Its Defect-Related Photoluminescence Properties. *Materials (Basel)* **2016**, *9*, 300. [[CrossRef](#)]
76. Bengas, R.; Lahmar, H.; Redha, K.M.; Mentar, L.; Azizi, A.; Schmerber, G.; Dinia, A. Electrochemical synthesis of n-type ZnS layers on p-Cu₂O/n-ZnO heterojunctions with different deposition temperatures. *RSC Adv.* **2019**, *9*, 29056–29069. [[CrossRef](#)]
77. Elsayed, E.M.; Shalan, A.E.; Rashad, M.M. Preparation of ZnO nanoparticles using electrodeposition and co-precipitation techniques for dye-sensitized solar cells applications. *J. Mater. Sci. Mater. Electron.* **2014**, *25*, 3412–3419. [[CrossRef](#)]
78. Chen, S.; Lin, L.; Liu, J.; Lv, P.; Wu, X.; Zheng, W.; Qu, Y.; Lai, F. An electrochemical constructed p-Cu₂O/n-ZnO heterojunction for solar cell. *J. Alloys Compd.* **2015**, *644*, 378–382. [[CrossRef](#)]
79. Li, Z.; Jia, M.; Doble, S.; Hockey, E.; Yan, H.; Avenoso, J.P.; Bodine, D.; Zhang, Y.; Ni, C.; Newberg, J.T.; et al. Energy Band Architecture of a Hierarchical ZnO/Au/Cu_xO Nanoforest by Mimicking Natural Superhydrophobic Surfaces. *ACS Appl. Mater. Interfaces* **2019**, *11*, 40490–40502. [[CrossRef](#)] [[PubMed](#)]
80. Iencinella, D.; Centurioni, E.; Grazia Busana, M. Thin-film solar cells on commercial ceramic tiles. *Sol. Energy Mater. Sol. Cells* **2009**, *93*, 206–210. [[CrossRef](#)]



© 2020 by the authors. Licensee MDPI, Basel, Switzerland. This article is an open access article distributed under the terms and conditions of the Creative Commons Attribution (CC BY) license (<http://creativecommons.org/licenses/by/4.0/>).